

## Article

# Potential for Energy Utilization of Air Compression Section Using an Open Absorption Refrigeration System

Bicui Ye <sup>1,2</sup>, Shufei Sun <sup>3</sup> and Zheng Wang <sup>1,\*</sup>

<sup>1</sup> School of Civil Engineering and Architecture, Zhejiang Sci-Tech University, Hangzhou 310018, China; yebicui73141@zstu.edu.cn

<sup>2</sup> School of Mechanical Engineering, Beijing Institute of Technology, Beijing 100081, China

<sup>3</sup> China National Air Separation Engineering Co., Ltd., Hangzhou 310051, China; sunshufei1988@126.com

\* Correspondence: zheng.wang@zstu.edu.cn; Tel.: +86-136-1652-0850

**Featured Application:** multi-stage compression process; low-grade waste heat recovery.

**Abstract:** In this paper, an open absorption refrigeration system is proposed to recover part of the waste compression heat while producing cooling capacity to further cool the compressed air itself. The self-utilization of the compression waste heat can significantly reduce the energy consumption of air compression, and hence increase the energy efficiency of the cryogenic air separation unit. To illuminate the energy distribution and energy conversion principle of the open absorption refrigerator-assisted air compression section, a thermodynamic model is built and the simulation work conducted based on a practical triple-stage air compression section of a middle-scale cryogenic air separation unit. Our results indicate that the energy saving ratio is mainly constrained by the distribution of the cooling load of compressed air, which corresponds to the heat load of the generator and cooling capacity of the evaporator in the open absorption refrigerator. The energy saving ratio ranges from 0.52–8.05%, corresponding to the temperature range of 5–30 °C and humidity range of 0.002–0.010 kg/kg. It is also estimated, based on the economic analysis, that the payback period of the open absorption refrigeration system is less than one year, and the net project revenue during its life cycle reaches USD 5.7 M, thus showing an attractive economic potential.

**Keywords:** open absorption refrigerator; waste compression heat; cryogenic air separation; thermodynamic and economic analysis



**Citation:** Ye, B.; Sun, S.; Wang, Z. Potential for Energy Utilization of Air Compression Section Using an Open Absorption Refrigeration System. *Appl. Sci.* **2022**, *12*, 6373. <https://doi.org/10.3390/app12136373>

Academic Editors: Xiaohong Han and Yingjie Xu

Received: 5 May 2022

Accepted: 20 June 2022

Published: 23 June 2022

**Publisher's Note:** MDPI stays neutral with regard to jurisdictional claims in published maps and institutional affiliations.



**Copyright:** © 2022 by the authors. Licensee MDPI, Basel, Switzerland. This article is an open access article distributed under the terms and conditions of the Creative Commons Attribution (CC BY) license (<https://creativecommons.org/licenses/by/4.0/>).

## 1. Introduction

Industrial gas plays an increasingly important role in the development of the economy. The market size of industrial gas in China grew rapidly from CNY 106.5 billion in 2016 to CNY 155.3 billion at the end of 2020, with an average annual compound growth rate of 10.5% [1]. The rapid growth of the industrial gas market has promoted the development of the cryogenic air separation unit (CASU), which remains the status quo for the industrial production of high-purity tonnage quantities of oxygen and nitrogen.

Gas production via CASU is a capital and energy-intensive process, mainly including an air compression section (ACS), purification, heat exchange, pre-cooling, rectification, and a storage process. Energy consumption of a CASU accounts for 15–20% of the total energy consumption in iron and steel enterprises [2]. Thus, a great effort has been made to reduce the energy demand and cost of the CASU. At earlier stages, efforts mainly focused on the reduction in pressure drops through the optimization of the purification system and distillation columns, and successfully reduced the specific energy consumption of liquid oxygen from 0.7 kWh/kg to around 0.4 kWh/kg [3,4]. Further effort has been made to improve the efficiency of compressors, as 70–80% of the overall power consumption of the CASU comes from the power requirement of feed air compressors [5]. Researchers found that a 19% reduction in specific power consumption could be achieved if the compressor

isentropic efficiency increased from 0.74 to 0.9 [6]. Efforts have also been made to optimize the system process through cold energy utilization from liquefied natural gas (LNG). Wu et al. [7] introduced a novel three-column CASU process integrated with LNG regasification, and reduced the specific power consumption of liquid oxygen and liquid nitrogen to 0.252 kWh/kg and 0.258 kWh/kg, respectively. Armin et al. [8] studied the integration of a CASU with LNG as a heat sink, and found an 8.04% reduction in the amount of power requirement, and a 17.05% reduction in the initial capital cost of the CASU plant. Through continuous development, molecular sieves for purification, booster expanders, and the structured packing of distillation columns for reducing pressure losses, have become relatively established, and the methods of improving compression efficiency through the optimization of design and control technology of the compressor impeller have approached their technical bottlenecks [9]. Consequently, researchers have turned their attention to the waste heat utilization from the ACS. During the ACS, feed air is compressed by double- or triple-stage compressors to 0.6–0.7 MPa, and the outlet air temperature of each stage reaches 100–120 °C. As a result, 90% of the compression consumption is lost as thermal energy of the compressed air [10]. Taking a CASU producing 120,000 Nm<sup>3</sup>/h oxygen as an example, the air compressor intake flow is about 600,000 Nm<sup>3</sup>/h, and the heat removed by cooling water is as high as 30 MW. At the same time, intercoolers have to be installed to cool down the compressed air to approximately 40 °C, with the aim of preventing a high suction temperature for the next stage of compression [11]. Therefore, the ACS is a high energy consumption process accompanied by considerable waste compression heat. On the other hand, a 40 °C suction temperature is too high for the compressors, thus leading to a large potential for a reduction in suction temperature, and compression power saving [12]. However, the waste compression heat is low-grade, with low energy density and strong volatility, which makes its recovery technically and economically challenging.

Methods of waste compression heat utilization that have been studied mainly include direct heat utilization and energy conversion methods. Direct heat utilization, though simple and effective, is limited by the lack of a suitable heat demand that can be matched with the waste compression heat in terms of amount and temperature grade [13]. To make better use of the low-grade compression heat, researchers have come up with energy conversion methods, which aim to compensate for part of the electricity or cooling demand of the CASU, and to realize the self-utilization of ACS.

Aneke M. et al. [14] proposed a direct binary cycle heat engine (ORC systems), which converted the waste compression heat to electricity and reduced the specific power consumption by an average of 11%. ORC has also been successfully applied in other process industries that produce waste compression heat, such as liquid air energy storage [15], combined heat and power systems [16], and oxy-combustion power plants [17]. Though they provide a valuable reference, these literature studies mainly focused on the thermodynamic characteristics of ORC itself, rather than the thermodynamic coupling principles between the ORC and the air compression process. The energy conversion from waste heat to electricity has been demonstrated to be an efficient way for energy utilization; however, some study results also show that the ORC power generation efficiency is significantly affected by the compression heat grade and its volatility [18], and may suffer from refrigerant leakage [19].

The electricity produced by ORC can also be further converted to the cooling capacity to satisfy the cooling demand of ACS. Rong et al. [20,21] investigated a cascade waste heat recovery system including dehumidification (DEH), ORC, and MR (DEH–ORC–MR), and found that 50% of the feed air humidity ratio can be decreased, which helped to increase the average isothermal efficiency of the compressors by about 5%. The waste compression heat utilization rate and energy saving rate reached 61.5% and 4.9%, respectively. Considering the possible problems caused by solute corrosion of DEH, Zhou et al. [22] studied an ORC–MR heat recovery system and obtained a maximum energy saving ratio of 4.2%. Thermoelectric cooling is another choice for converting electricity to the cooling capacity. Though it has advantages of being compact in size, light in weight, of high reliability,

and with no mechanical moving parts, no working fluid [23,24], it is more frequently applied for small-scale cooling demand, such as domestic and portable refrigerators [25], laboratory and scientific equipment cooling, i.e., laser diodes or integrated circuit chips [26], automobile mini-refrigerators, and thermoelectric cooler/heaters in car seats [27].

Researchers have also proposed heat-driven systems to realize the conversion of waste compression heat to cooling capacity directly. Zhu et al. [28] proposed a waste heat-driven vacuum fiber membrane dehumidification (VFMD) system, which improved the working condition the of compressors by dehumidifying the feed air, and recovered 55.1% of the waste compression heat. Du et al. [29] conducted a study on an absorption refrigerator (AR) with combined ACS, and found that 68.7% of the cooling water could be saved in the ACS. Zhi et al. [30] coupled an AR with a DEH system via a shared regenerator to achieve both the cooling and dehumidification of the suction air of the compressors. Although AR and ORC have been widely accepted and applied as effective ways to recover low-grade waste heat, their applications in the CASU are still in the proof-of-concept stage. Furthermore, as shown in Figure 1, the waste heat-driven temperature of the ORC and AR lies between 90–150 °C [31], while the exhaust temperature of compressed air is about 110–120 °C, which means that the available driven temperature is between 90–120 °C, leaving a larger temperature difference (at least 40–90 °C) for the cooling capacity. Obviously, there is a mismatch between the cooling capacity and driving heat, which has to be compensated for by intermediate heat sinks. This requires a large heat recovery and utilization system, with consequent high cost and complex operation.

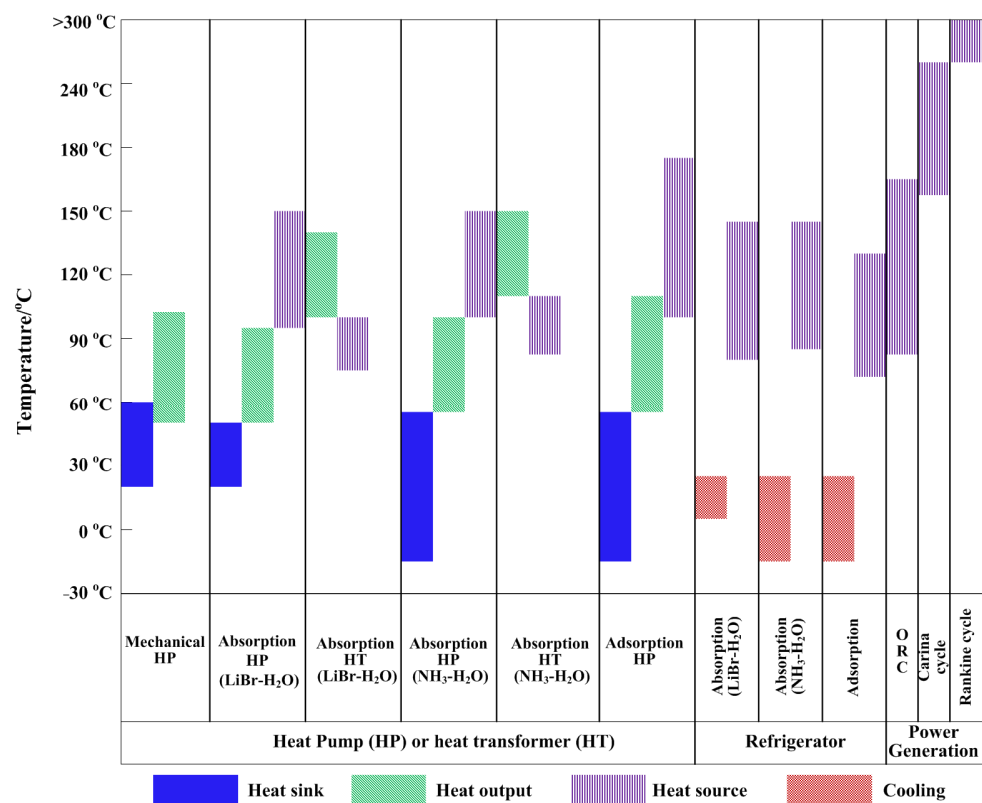


Figure 1. Typical applicable temperature ranges of different conversion technologies of waste heat [31].

This study proposes a simpler structured open absorption refrigerator (OAR) to solve this problem, as the OAR can have a fairly low-temperature refrigeration effect, at a much smaller temperature difference between the heat source and heat sink, compared to the close absorption refrigerator (CAR) [32]. It can be driven by waste compression heat as low as 55 °C, which means that the available waste heat-driven temperature is between

55–120 °C, leaving a much smaller temperature difference for the cooling demand. As a result of the strong match between the driving heat and cooling capacity, no intermediate heat sinks are required. It also makes it possible to achieve an evaporation temperature of the OAR as low as 15 °C, which can further satisfy the pre-cooling demand before the molecular sieve stage. Therefore, an OAR theoretically has a considerable energy saving and consumption reduction effects, with a much lower initial and operation cost compared with existing technologies. Although the OAR system has been studied for solar energy utilization, most of the studies on OAR have focused on the system itself, or on the efficiency of the solar collector [33]. The coupling of OAR with the ACS (ACS–OAR) to realize the self-utilization of waste compression heat has not yet been reported, which is the first novelty this paper addresses.

The energy conversion between the ACS and OAR is closely coupled with the waste compression heat and cooling capacity of the OAR. They are also constrained by each other due to the strong relationship between the compressed air temperature and the evaporation temperature of the OAR and the cooling capacity distribution. Thus, the scientific challenge of the coupling of an OAR with an ACS system lies in the internal waste heat distribution principle between the multi-stage compression process, and the internal energy conversion principle between the waste compression heat and cooling capacity of the OAR. Another challenge arises due to the changeable conditions of feed air, and the consequent transient operating conditions of the ACS–OAR. Thus, it is crucial to carry out studies on the off-design performances under a wide range of operating parameters, which would help to establish a reliable and efficient prediction, regulation, and control method. This is the second novelty this paper addresses.

## 2. Materials and Methods

Figure 2 shows a schematic diagram of the conventional ACS in a CASU (Figure 2a), and a diagram of an ACS coupled with an OAR system (Figure 2b).

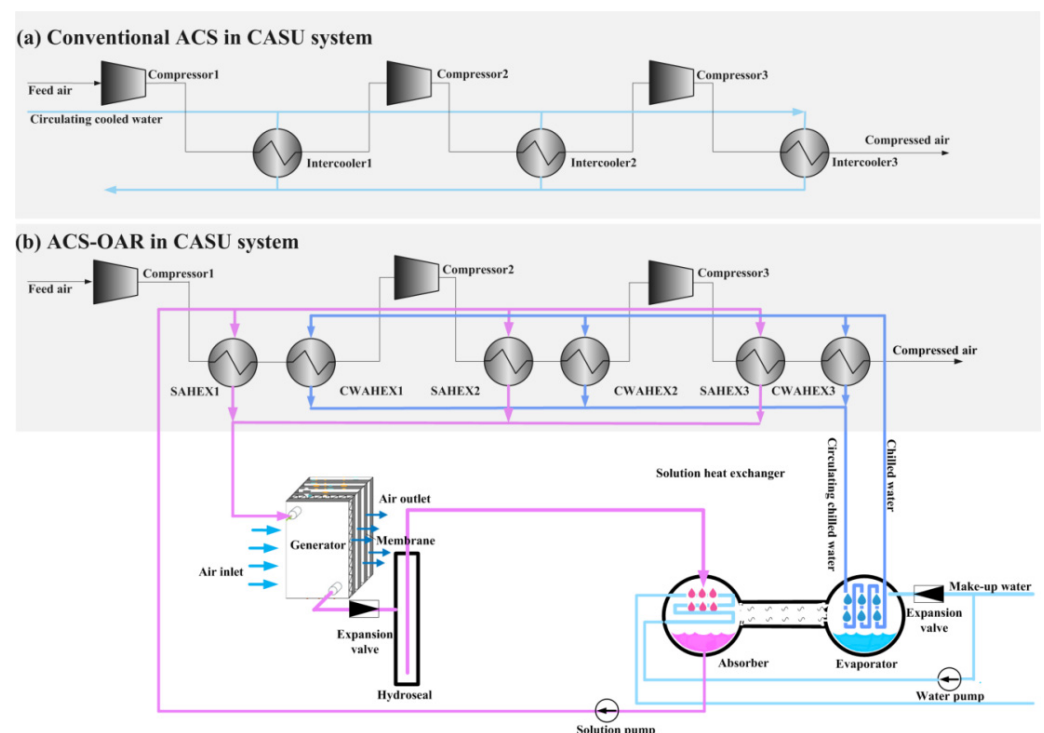


**Figure 2.** (a) Schematic of a feed air compression section with conventional cooling system; (b) schematic of a cryogenic air separation unit coupled with an open-cycle absorption refrigerator.

### 2.1. Conventional Air Compression Section

As shown in Figure 2a, the feed air is compressed to 0.6–0.7 MPa by triple-stage compressors. The outlet air temperature of each compressor reaches 100–120 °C. To prevent high suction temperature of the compressors, intercoolers with a cooling water loop are installed, and reduce the air temperature to 40 °C. Cooling water in the intercoolers is provided by an air-cooling tower (ACT1) at about 32 °C. After the ACS, compressed air has to be pre-cooled below 17 °C (the limitation temperature for the molecular sieve in the purification process) in a lower temperature air-cooling tower (ACT2). Chilled water in the ACT2 comes from a water-cooling tower (WCT), in which waste nitrogen is used to produce the chilled water at 11 °C. Some sulfide impurities in the air can also be removed in the WCT. Afterwards, the pre-cooled compressed air flows into the molecular sieve for further purification, in which water, carbon dioxide, hydro-carbons and other contaminants are removed. Then, the compressed air is cooled to cryogenic temperatures (from –168 °C to –196 °C) by the backflow of products, before it is separated into useful products in the distillation columns [11].

### 2.2. Air Compression Section Coupled with OAR System

As shown in Figure 2b, solution-air heat exchangers (SAHEXs) and a cooling water-air heat exchangers (CWAHEXs) are present in each compressor. The compressed air is first pre-cooled by solution in the SAHEXs, and then further cooled to the target temperature by chilled water in the CWAHEXs. Solution in the SAHEXs comes from the absorber of the OAR, and chilled water in the CWAHEXs comes from the evaporator of the OAR.

Three SAHEXs, an open generator, an absorber, an evaporator, two throttle valves, and a solution pump comprise of the OAR system. This system produces chilled water during the evaporation process, occurring in the evaporator, where water is sprayed externally, evacuates at a low pressure, and undergoes flash evaporation into water vapor. Chilled water produced in the evaporator flows into the CWAHEXs to further cool the compressed air to a relatively low temperature. Water vapor created in the evaporator flows into the absorber and is absorbed by the strong solution. The continuous absorption of water vapor maintains a low pressure in the evaporator and absorber. A cooling water loop takes away the absorption heat. The solution becomes diluted during the absorption process, and is collected at the bottom of the absorber before being pumped into the SAHEXs. Temperature of the diluted solution increases by exchanging heat with the compressed air in the SAHEXs. Then, solution from SAHEXs flows into the open generator, where water vapor in the diluted solution is transferred to the atmospheric air due to the water vapor partial pressure difference between the solution and air. Strong solution is collected at the bottom of the open generator and flows back to the absorber through a throttle valve, thus completing the OAR cycle.

To better illustrate the advantage of the proposed cycle, p-T-x diagrams of the OAR cycle and CAR cycle are compared under the same working condition, as shown in Figure 3. The red line represents the OAR system, while the blue line represents the CAR system. The solid line, dashed line, and dot line represent the liquid flow, vapor flow, and compressed air flow, respectively.

As can be seen from Figure 3, it takes three steps for the CAR system to cool the compressed air (purple line). An intermediate cooler has to be installed to compensate for the mismatch between the driving heat and cooling capacity, as explained in the introduction section. It takes only two steps for the OAR system, the first of which occurs in the SAHEXs, while the second occurs in the CWAHEXs (orange line). As the OAR can be driven by waste compression heat as low as 55 °C, the driving heat load can be well matched with the cooling demand of the CWAHEXs, as well as the cooling capacity of the OAR. As a result, no intermediate heat sinks are required; also, an evaporation temperature as low as 15 °C can be achieved. Waste heat obtained from SAHEXs is used to drive the OAR to produce continuous cold energy. In addition, the low evaporation temperature is also helpful for removing the WCT and ACT2 before the molecular sieve stage. Although

ACT1 is still required for the absorber of the OAR system, the cooling load of ACT1 for the OAR is much lower than the cooling load of ACT1 for the conventional cooling water loop, as the former deals with the cooling load of compressed air from 45 to 17 °C, while the latter deals with the cooling load of compressed air from 110 to 40 °C.

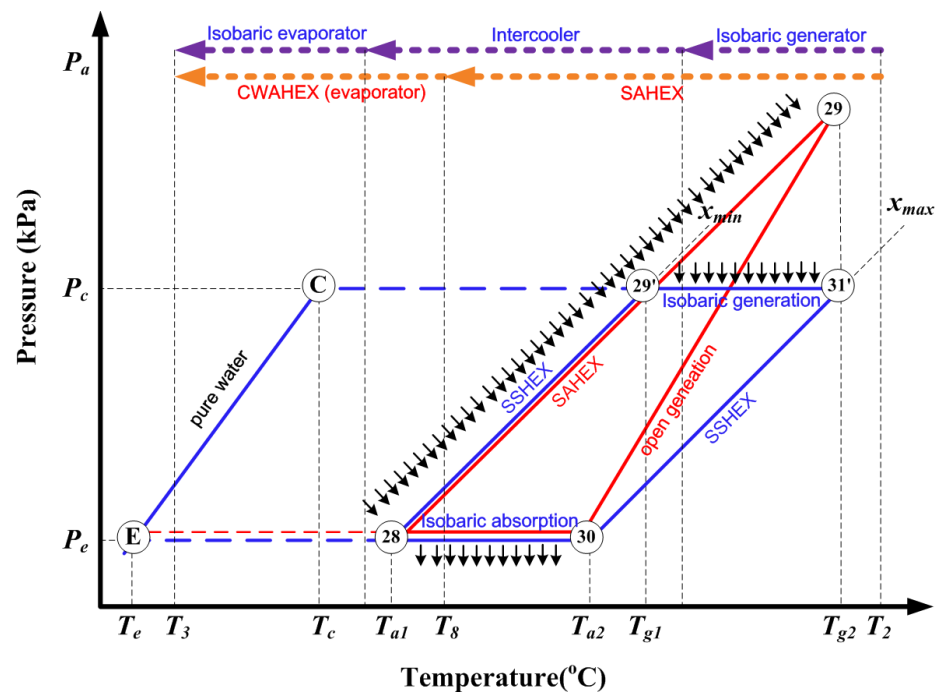


**Figure 3.** Schematic of a cryogenic air separation unit coupled with an open-cycle absorption refrigerator.

On the other hand, a lower evaporation temperature means lower suction temperatures, which is beneficial for the energy saving and performance enhancement of compressors. Hence, compared to CAR, the OAR system has the advantages of a simpler structure and less supplementary heat sinks. However, the energy conversion between the ACS and OAR is closely coupled to the waste heat and cold energy in the forms of energy quantity and quality (temperature), forming a complicated constrained energy flow feedback loop. Thus, the energy distribution principle and energy conversion principle between the multi-stage waste compression heat and cooling capacity of the OAR under different working conditions will be discussed to demonstrate the feasibility of the ACS–OAR system. The profitability will also be analyzed.

### 2.3. Modeling

To quantitatively investigate the performance of the ACS–OAR system, detailed analyses are carried out through calculation. In this section, the methodology for performance calculation will be introduced, including the assumptions, parameter definitions, and thermophysical property calculation. The following assumptions are made to simplify the model:

- The system operates under steady state.
- The heat losses of the devices and pipes are ignored.
- Pressure drops in pipes are neglected.
- Pressures of the absorber and evaporator are the same.
- Solution is saturated at the outlet of the open generator and absorber. Water vapor is saturated at the outlet of the evaporator.
- Heat and mass transfer in the open generator only occur between the liquid and gas phase.
- No condensation occurs in the compression process.

As one of the most widely used absorbent solutions for absorption refrigerators, LiBr-H<sub>2</sub>O is selected as the working absorbent in this study. Properties of LiBr-H<sub>2</sub>O are provided by Refprop 9.0. It should be noted that the retrofit of the CASU only takes place in the ACS, and there will not be any change in the operating conditions of the purification and distillation sections.

### 2.3.1. Modeling of the Air Compression Section

Triple-stage compression will be analyzed in this case. Processed parameters of the triple-stage air compression section are shown in Table 1.

**Table 1.** Processed parameters in the triple-stage air compression section.

Parameters	Triple-Stage
Components of feed air	Nitrogen 0.7812; Oxygen 0.2095; Argon 0.0093
Feed air mass flow rate (kg/h)	340,439.85
Product (kg/h)	
Liquid O <sub>2</sub> (0.3 MPa, −183 °C)	2992.78
Gas O <sub>2</sub> (2.82 MPa, 20 °C)	71,381.73
Liquid N <sub>2</sub> (0.6 MPa, −189.3 °C)	2499.67
N <sub>2</sub> (0.524 MPa, 20 °C)	56,240.97
N <sub>2</sub> (0.114 MPa, 20 °C)	31,245.44
N <sub>2</sub> (1 MPa, 40 °C)	56,242.79
Outlet pressures of compressors (kPa)	
Compressor I	200
Compressor II	360
Compressor III	635
Isentropic efficiency of compressors	85%
Pressure drop of each inter and after coolers (kPa)	8
Outlet temperatures of intercoolers and aftercooler (°C)	
Intercooler I	40
Intercooler II	40
Aftercooler I	40
Variables	
Inlet air temperature of feed air (°C)	13.8–25
Inlet air mass fraction of water (kg/kg)	0.06–0.016

Power consumption of air compression is calculated as:

$$T_{aout} = T_{ain}(1 + (1/\eta_{comp}) \times (r_c^{R/c_{pa}} - 1)) \quad (1)$$

$$h_{fa} = 1.01t_{fa} + 0.01d_{fa}(2501 + 1.85t_{fa}) \quad (2)$$

$$W_{comp} = m_{fa}(h_{faout} - h_{faain}) / (1 + d_{fa}) \quad (3)$$

$$W_{comp} = \frac{\gamma_c}{\gamma_c - 1} \cdot \frac{mRT_{in}}{\eta_{comp}} \left[ \left( \frac{p_{out}}{p_{in}} \right)^{\frac{\gamma_c}{\gamma_c - 1}} - 1 \right] \quad (4)$$

where  $r_c$  represents compression ratio, %;  $\eta_{comp}$  represents isentropic efficiency of compressors, %;  $d$  is absolute humidity of feed air, kg/kg;  $W_{comp}$  represents power consumption of compressors, kW. Subscript “fa” represents the feed air. Subscripts “faain” and “faout” of  $T$  and  $h$  represent feed air inlet and outlet of each stage compressor.

### 2.3.2. Modeling of OAR System

Modeling of OAR system includes the evaporator, open generator, absorber, and SAHEXs and CWHEXs.

(1) Evaporator and absorber

The evaporator and absorber are both considered as shell-and-tube heat exchangers. Chilled water for the evaporator and cooling water for the absorber flow through the tube side. Makeup water evaporation and water vapor absorption occur at the shell side. It is solved by the simple effectiveness–number of transfer units ( $\epsilon$ - $NTU$ ) model:

$$NTU_{eva} = (UA)_{eva} / (m_{clw}c_{p,clw}) \tag{5}$$

$$\epsilon_{eva} = 1 - \exp(-NTU_{eva}) \tag{6}$$

$$\epsilon_{eva} = (t_{clwin} - t_{clwout}) / (t_{clwin} - t_{eva}) \tag{7}$$

The same calculation method is adopted for the absorber.

The evaporation rate of the makeup water gives a direct measure of the cooling capacity of the OAR. The energy conservation equation is given:

$$m_{mw}(h_{mwin} - h_{mwout}) = m_{clw}(h_{clwin} - h_{clwout}) \tag{8}$$

where  $U$  represents the heat transfer coefficient,  $W/(m^2 \cdot K)$ ;  $A$  represents heat transfer area,  $m^2$ ;  $c_p$  represents the specific heat capacity,  $J/(kg \cdot K)$ ; subscripts “ $clw$ ” and “ $mw$ ” represent chilled-water and makeup water, respectively.

Mass and energy conservation equations for the absorber are given as:

$$(mx)_{ssin} = (mx)_{ssout} \tag{9}$$

$$m_{ssin} + m_{mw} = m_{wsout} \tag{10}$$

$$(mh)_{mwin} + (mh)_{ssin} - (mh)_{wsout} = m_{cw}(h_{cwout} - h_{cwin}) \tag{11}$$

where  $x$  represents mass fraction of solvent in the solution, %; subscripts “ $ws$ ”, “ $ss$ ” and “ $cw$ ” represent weak solution, strong solution, and circulating cooling water, respectively.

(2) SAHEXs and CWHEXs

A shell-and-tube heat exchanger is used here, in which solution flows through the tube side, while air flows through the shell side. Air and solution temperatures are also solved by the counterflow  $\epsilon$ - $NTU$  model:

$$NTU_{SAHEX} = (UA)_{SAHEX} / \min(m_{ws}c_{pws}, m_a c_{pa}) \tag{12}$$

$$\epsilon_{SAHEX} = \frac{1 - \exp\left((-NTU_{SAHEX})\left(1 - \frac{\min(m_a c_{pa}, m_{ws} c_{pws})}{\max(m_a c_{pa}, m_{ws} c_{pws})}\right)\right)}{1 - \frac{\min(m_a c_{pa}, m_{ws} c_{pws})}{\max(m_a c_{pa}, m_{ws} c_{pws})}\left((-NTU_{SAHEX})\left(1 - \frac{\min(m_a c_{pa}, m_{ws} c_{pws})}{\max(m_a c_{pa}, m_{ws} c_{pws})}\right)\right)} \tag{13}$$

$$\epsilon_{SAHEX} = \frac{\max(t_{ain} - t_{aout}, t_{wsout} - t_{wsin})}{t_{ain} - t_{wsin}} \tag{14}$$

The energy conservation equation is given as:

$$(mh)_{wsin} + (mh)_{fain} = (mh)_{wsout} + (mh)_{faout} \tag{15}$$

The same calculation method is adopted for CWAHEXs. It is worth noting that pressure drops of SAHEXs and CWAHEXs are all assumed to be 4 kPa due to the similar patterns.

(3) Open generator

According to the mass conservation, the mass flow rate of water vapor driven out from the diluted solution in the generator is equal to the mass flow rate of makeup water evaporated in the evaporator, which determines the cooling capacity of the OAR. Thus, the generation performance of the open generator is a key measurement of the system cooling

capacity. An adiabatic, counterflow, plate-and-frame membrane energy exchanger (MEE) is adopted as the open generator to prevent corrosion. The solution channel and air channel are separated by a microporous membrane. Water vapor in the solution channel transfers to the air channel through the microporous in the membrane. Geometric parameters and properties of the membrane, as well as the parameters of the MEE, are given in Table 2 [34].

**Table 2.** Geometric parameters of the membrane generator.

Properties		Unit	Value
Membrane thickness	$\theta_m$	$\mu\text{m}$	60
Membrane porosity	$\varepsilon$	%	75
Membrane pore diameter	$dp$	$\mu\text{m}$	1.0
Tortuosity factor	$\chi$		$(2 - \varepsilon)2/\varepsilon$
Membrane thermal conductivity	$\lambda$	$\text{W}/(\text{m}\cdot\text{K})$	0.25
Channel Length	$L$	mm	200
Channel Width	$W$	mm	200
Depth of solution channel	$\theta_s$	mm	0.16
Depth of moist gas channel	$\theta_g$	mm	1

One membrane and two neighboring flow channels are selected as the calculation domain, which is discretized into 200 segments along the flow direction. Mass transfer in each segment is described as:

$$m_v^i = J^i(w \cdot dz) \tag{16}$$

$$J^i = K^i(p_{av}^i - p_{sv}^i) \tag{17}$$

where  $m_v$  is the mass flow rate of water vapor, kg/s;  $w$  and  $dz$  represent the width of the solution channel and length of each segment, respectively, m;  $p_{av}^i$  and  $p_{sv}^i$  are the water vapor partial pressure of atmospheric air and solution, respectively, kPa;  $K^i$  represents the overall mass transfer coefficient,  $\text{kg}/(\text{m}^2\cdot\text{s})$ , which can be expressed as:

$$\frac{1}{K^i} = \frac{1}{k_{air}^i} + \frac{\delta}{k_m} \tag{18}$$

where  $k_{air}^i$  is the convective mass transfer coefficient of the air side,  $\text{kg}/(\text{m}^2\cdot\text{s})$ , and  $k_m$  is the permeability of the membrane,  $\text{kg}/(\text{m}\cdot\text{s})$ .

The solution channel in each element is considered as a control volume, and the mass conservation equations in each element are given as:

$$m_s^{i+1} = m_s^i + m_v^i \tag{19}$$

$$m_a^{i+1} = m_a^i - m_v^i \tag{20}$$

$$x_s^{i+1} = x_s^i \cdot m_s^i / m_s^{i+1} \tag{21}$$

Heat transfer in the differential element is also described:

$$U^i(T_s^i - T_a^i)wdz = m_v^i h_v^i - m_s^i c_{ps}^i dT_s^i \tag{22}$$

$$U^i(T_s^i - T_a^i)wdz = m_a^i c_{pa}^i dT_a^i \tag{23}$$

where  $U^i$  is the overall heat transfer coefficient,  $\text{W}/(\text{m}^2\cdot\text{K})$ . This can be expressed as:

$$\frac{1}{U^i} = \frac{1}{u_a^i} + \frac{\theta_m}{\lambda_m^i} + \frac{1}{u_s^i} \tag{24}$$

where  $u_a^i$  and  $u_s^i$  are the convective heat transfer coefficients of the air and solution side, respectively,  $\text{W}/(\text{m}^2\cdot\text{K})$ ;  $\lambda_m^i$  is the thermal conductivity of membrane,  $\text{W}/(\text{m}\cdot\text{K})$ . It is

assumed that air and solution flow are fully developed laminar flow and constant heat flux with Reynolds numbers much less than 2300. Thus, convective heat and mass transfer coefficients are calculated by the equations below:

$$Nu = \frac{uD_h}{\lambda} \quad (25)$$

$$Sh = \frac{k_m D_h}{D_f} \quad (26)$$

where  $D_h$  is the hydraulic diameter of the flow channel, and is calculated as  $D_h = 2A_c/(a + b)$ ;  $\lambda$  is the thermal conductivity of the fluid, W/(m·K);  $D_f$  is the diffusivity of water vapor, m<sup>2</sup>/s. Fully developed Nusselt and Sherwood numbers for the two fluids under different aspect ratios (ratio of channel width to channel height) are taken from [34].

### 2.3.3. Performance Metrics

Part of the waste compression heat is recovered and utilized by the OAR system. It is calculated as:

$$Q_{WHU} = Q_{SAHEX1} + Q_{SAHEX2} + Q_{SAHEX3} \quad (27)$$

The rest of the waste compression heat is equal to the cooling capacity of the OAR:

$$Q_{CLOAR} = Q_{CWAHEX1} + Q_{CWAHEX2} + Q_{CWAHEX3} \quad (28)$$

Thus, the waste heat recovery ratio can be calculated as:

$$WHRR = \frac{Q_{WHU}}{Q_{WHU} + Q_{CLOAR}} \quad (29)$$

The coefficient of performance (COP) of the OAR system is calculated as:

$$COP = \frac{Q_{CLOAR}}{Q_{WHU}} \quad (30)$$

Total power consumption for the air compression section of new ( $ACS_n$ ) and conventional CASU systems ( $ACS_c$ ) is calculated as:

$$W_{ACS_n} = W'_{comp1} + W'_{comp2} + W'_{comp3} \quad (31)$$

$$W_{ACS_c} = W_{comp1} + W_{comp2} + W_{comp3} \quad (32)$$

Energy saving ratio is calculated as:

$$ESR = \frac{W_{ACS_c} - W_{ACS_n}}{W_{ACS_c}} \quad (33)$$

It must be noted that pump and fan power consumption in ACT and WCT are neglected in the calculation of  $W_{ACS_n}$  and  $W_{ACS_c}$  because the ESR and payback period are calculated based on the power consumption difference between  $ACS_c$  and  $ACS_n$ . Compared to the  $ACS_c$ , the  $ACS_n$  spares the power consumption for ACT2 and WCT due to the low evaporation temperature of the OAR, while, in return, increases the power consumption of the solution pumps and fans of the OAR. Thus, the power consumption difference of the pumps and fans between the  $ACS_c$  and  $ACS_n$  are relatively small compared with the power consumption for air compression.

### 2.3.4. Economic Analysis

Economic calculation of the proposed ACS–OAR is also conducted to evaluate its profitability. Economic evaluation is based on the dynamic payback period (DPP), which is widely used for financial evaluation of investment.

The calculation of  $DPP$  is based on the annualized cost of system ( $C_{acs}$ ), which is comprised of annualized capital cost, maintenance cost, management cost, and operation cost:

$$C_{acs} = C_{acc} + C_{ama} + C_{amg} + C_{aop} \tag{34}$$

where, annualized capital cost of the system is calculated as:

$$C_{acc} = C_{dcc} \cdot \alpha = C_{dcc} \frac{i(i+1)^n}{(i+1)^n + 1} \tag{35}$$

where  $\alpha$  represents capital recovery ratio, also known as the amortization ratio, which is a function of the interest rate  $i$  and estimated lifetime of the proposed system  $n$ .  $C_{dcc}$  is the direct capital cost. It is worth noting that economic analysis is conducted based on the increased capital cost of the ACS caused by the coupling of OAR compared with conventional ACS. Accordingly,  $C_{dcc}$  is calculated as:

$$C_{dcc} = (C_{dcc})_{ACS-OAR} - (C_{dcc})_{CACS} = \sum_{i=1}^k (C_i)_{ACS-OAR} - \sum_{i=1}^k (C_i)_{CACS} \tag{36}$$

Direct capital costs of the ACS includes purchase costs of the main equipment, pipes and fittings, control devices, and so on. Purchase cost of the main equipment, such as the evaporator, open generator, and heat exchangers, are usually estimated by the production capacity index approach. Equations and references adopted are given in Table 3.

**Table 3.** Calculation of initial capital cost of the main system equipment [35–38].

Equation	
Absorber	
Evaporator	$C_{hex} = f_m \cdot 1192 \cdot (A_{hex})^{0.71}$
Solution heat exchanger	$A_{hex} = \frac{Q_{hex}}{U_{hex}(LMTD)_{hex}}$
SA-HEX1/2	$f_m$ : Material factor
CWA-HEX1/2	$LMTD$ : Mean logarithmic temperature difference
Intercooler	$U_{hex}$ : overall heat transfer coefficient
Aftercooler	
Pumps and blowers	$C_{pump} = 2100 \left( \frac{W_{pump}}{10} \right)^{0.26} \left( \frac{1 - \eta_{is,pump}}{\eta_{is,pump}} \right)^{0.5}$
Compressors	$C_{comp} = 71.1 \left( \frac{m_{comp} CR}{0.01} \right) \ln(CR)$
Expansion valves	$C_{ev} = 114.5 \cdot m_{ev}$
Air-cooling tower	$C_{tower} =$
Water-cooling tower	$1780H^{0.87} d^{1.23} [2.86 + 1.694f_m(10.01 - 7.408 \ln P + 1.395(\ln P)^2)]$
	$H$ : Height of the column; $d$ : Diameter of column $f_m$ : Material factor; $P$ : Column mean pressure

The management cost is considered annually as 20% of the operating labor cost. The maintenance cost is set annually as 4.63% of the capital investment cost [33]. Annualized operation cost in the ACS–OAR mainly consists of fresh water, electricity, and labor cost.

Based on the annualized capital cost,  $DPP$  is calculated as:

$$NPV = -C_{dcc} + \sum_{t=0}^{DPP} \frac{(P_r - C_{acs})(1 - T_r)}{(1 + D_r)^t} = 0 \tag{37}$$

where  $NPV$  (net present value) is the present value of the current and future benefit minus the present value of the current and future costs, which is a base calculation for the  $DPP$ ;  $T_r$  and  $D_r$  are the tax rate and discounted annual rate, respectively, %.  $P_r$  is the project revenue, which refers to the value created by the energy saving caused by the coupling

of the OAR in the ACS, USD. The energy saving mainly refers to the electricity saving of compressors. The value of electricity saving is calculated as:

$$P_r = \Delta W_{com} \cdot wh \cdot EP \tag{38}$$

where  $\Delta W_{com}$  is the electricity saving, kW;  $wh$  is the working hours of the system, h;  $EP$  is the electricity purchase price, USD/kWh.

### 2.3.5. Calculation Procedure

Based on the simulation model and performance metrics, the thermodynamic characteristics of the ACS–OAR system were calculated as the following procedures (shown in Figure 4). An appropriate code was developed and implemented in the MATLAB® environment (R2019b, MathWorks, Hangzhou, China).

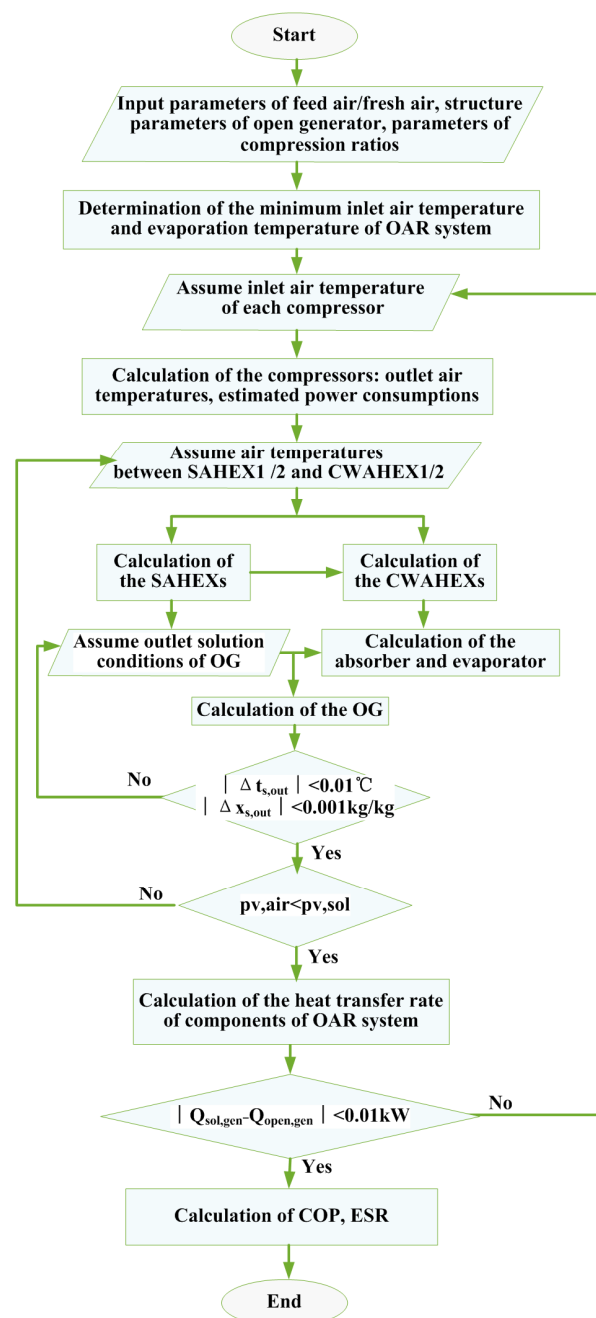


Figure 4. Calculation procedure of the model.

### 3. Results

Simulation results of the ACS–OAR system, based on the working conditions of the ACS in Table 1, are discussed in this section. Firstly, validation is conducted to verify the accuracy of the model. Thereafter, optimization of the system, parametric sensitivity, and economic analysis are discussed under different working conditions.

#### 3.1. Validation

To verify the calculation results of the proposed ACS–OAR system, a validation procedure was conducted to compare our results with the work in the literature. Based on the author’s knowledge, the ACS–OAR system investigated here has not yet been reported. Accordingly, the ACS and OAR system have to be validated separately. The work of Aneke et al. [14] was selected here to validate the ACS system model, and the work of Al-Shafei et al. [32] was selected to validate the OAR system model. Validation results are listed in Table 4. It can be seen that the deviation between the calculated results of this work and the data in the literature is less than 5%, which is acceptable and verifies the accuracy of the model.

**Table 4.** Model verification of simulation results with reported results.

	This Work	Literature [14]	Error		This Work	Literature [32]	Error
Temperature at the outlet of compressor I (°C)	109	106.3	0.025	Generation heat (kW)	13,214	12,732	0.036
Pressure at the outlet of compressor I (kPa)	198	200.6	−0.013	Evaporation heat (kW)	9102	8966	0.015
Temperature at the outlet of compressor II (°C)	107	104.9	0.019	Absorption heat (kW)	11,605	11,033	0.049
Pressure at the outlet of compressor II (kPa)	346	360	−0.038	Mass concentration of strong solution	51.22%	50.66%	0.011
Temperature at the outlet of compressor III (°C)	113	109.7	0.039	Outlet temperature of strong solution (°C)	40.6	39.26	0.033
Pressure at the outlet of compressor III (kPa)	635	635	0				
Power consumption of compressors (kW/kg)	222	216	0.027				

#### 3.2. Optimization of the Suction Temperature

As can be deduced from Equations (4) and (33), the suction temperatures of the compressors are the most direct parameters that determine  $ESR$  at a given compression ratio, and further determine the overall cooling load of the compressed air. Thus, we first analyzed the optimization of the suction temperatures under different working conditions.

Firstly, to avoid water condensation in the compressors, which is harmful to the compressor operation, a minimum suction temperature ( $ST_{min}$ ) must be established, defined as the air temperature with 90% relative humidity. As shown in Figure 5a, the minimum suction temperature of each compressor increases with the air humidity and pressure. It can be deduced that the  $ST_{min}$  in humid areas is higher than the suction temperatures in dried areas. The highest  $ST_{min}$  over a year usually occurs in July or August, the most humid months (Figure 5b). As long as the  $ST_{min}$  is higher than the cooling water temperature, water condensation of the compressed air occurs, which is inevitable even when 40 °C intercoolers are adopted; thus, adequate drainage must be ensured to minimize the damage to the compressors.

Operation parameters, such as the evaporation temperature ( $T_{eva}$ ), the solution-to-air flow ratio in the generator ( $FR_{s-a}$ ), suction temperature of each compressor ( $ST_{com}$ ), and approach temperatures of SAHEXs ( $AT_{sahex}$ ) can be optimized to adjust the cooling load allocation. Thus, we varied  $AT_{sahex}$  from 10 to 24 °C,  $T_{eva}$  from 10–14 °C, and  $FR_{s-a}$  from 2 to 5, and calculated the corresponding  $ST_{com}$ , as show in Figure 6a–d.

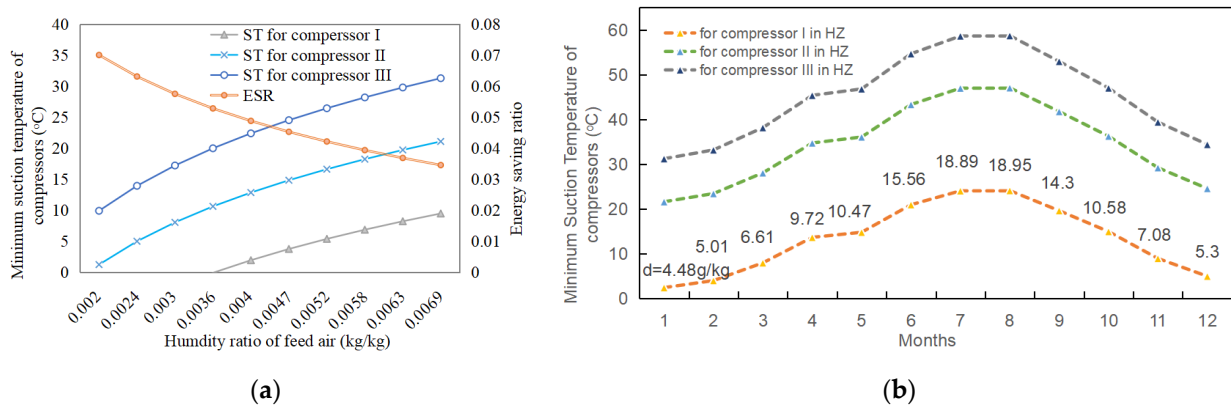


**Figure 5.** (a) Minimum suction temperature of each compressor under different feed air humidity; (b) Minimum suction temperature for each compressor in different months in Hangzhou. However, without external heat or electricity sources, the  $ST_{min}$  cannot always be achieved. It is constrained by the cooling load allocation between SAHEXs ( $Q_{sahexs}$ ) and CWAHEXs ( $Q_{cwahexs}$ ).  $Q_{sahexs}$ , which provides the generation heat of the OAR, and  $Q_{cwahexs}$ , which is provided by the evaporation heat of the OAR, have to be distributed carefully to obtain enough generation heat while ensuring adequate cooling capacity for air cooling.

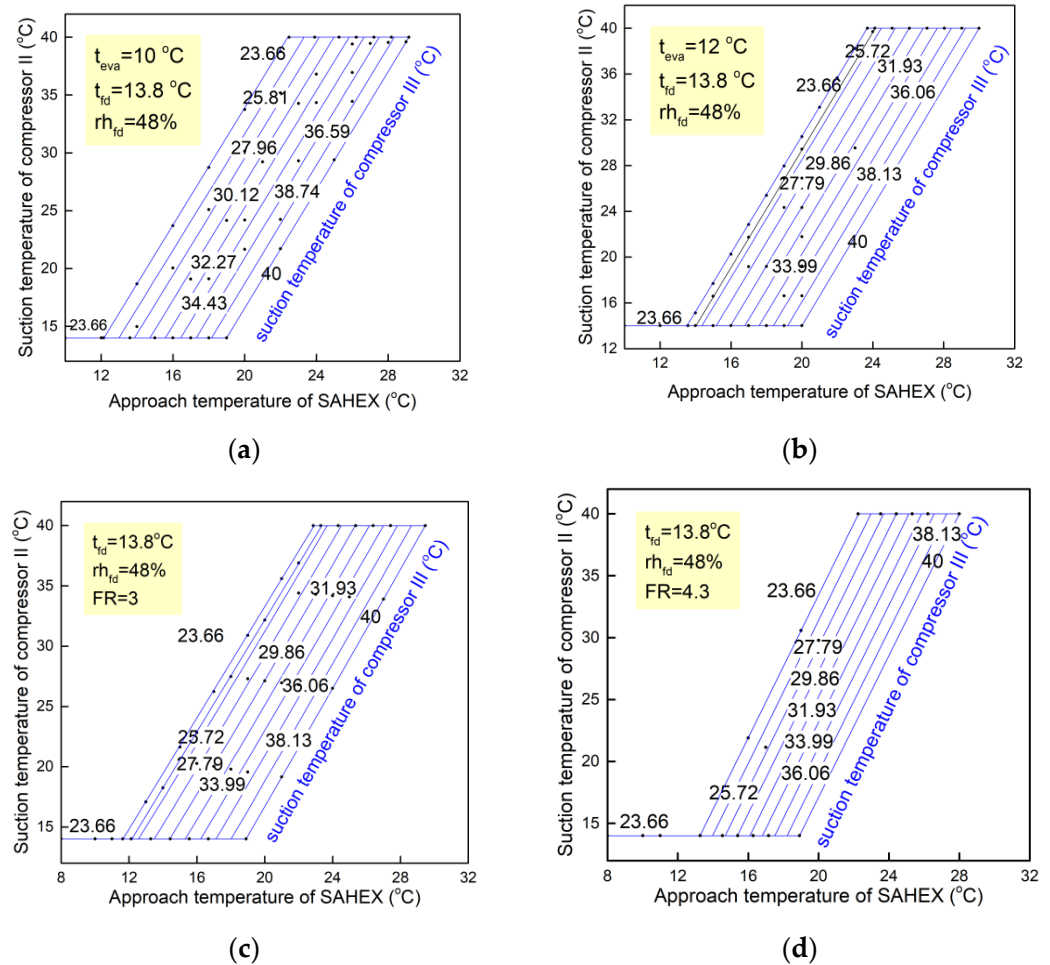


**Figure 6.** Optimization of suction temperatures of compressors under different working conditions: (a)  $T_{eva} = 10\text{ °C}$ ,  $FR_{s-a} = 2.3$ ; (b)  $T_{eva} = 12\text{ °C}$ ,  $FR_{s-a} = 2.3$ ; (c)  $T_{eva} = 12\text{ °C}$ ,  $FR_{s-a} = 3$ ; (d)  $T_{eva} = 12\text{ °C}$ ,  $FR_{s-a} = 4.3$ .

In Figure 6, suction temperatures of compressor II ( $ST_{com2}$ ) and III ( $ST_{com3}$ ) vary from 14.01 to 40 °C and 23.66 to 40 °C, respectively, at a given suction temperature (13.8 °C) of compressor I, which is equal to the feed air temperature. Figure 7 indicates an inverse relationship between the  $ST_{com2}$  and  $ST_{com3}$ . This can be explained as follows: The decrease in  $ST_{com2}$  leads to the increase in the cooling load of CWAHEX1 and a decrease in the cooling load of SAHEX2, while CWAHEX3 and SAHEX1 remain unchanged. In addition,  $ST_{com3}$  has to be raised to increase the cooling load of SAHEX3 and decrease the cooling load of CWAHEX2, to establish a new cooling load balance between the SAHEXs and CWAHEXs, which is also an energy balance between the generation heat and evaporation heat of the OAR. The effects of  $AT_{sahex}$  on the determination of suction temperatures can also be observed in Figure 7. The minimum  $ST_{com2}$  (14.01 °C) and  $ST_{com3}$  (23.66 °C) can be simultaneously achieved only when the  $AT_{sahex}$  is below a minimum value ( $AT_{sahex,min}$ ). With an  $AT_{sahex}$  smaller than  $AT_{sahex,min}$  (solid line in Figure 7,  $AT_{sahex} = 10$  °C), the SAHEXs undertake a greater cooling load of the compressed air, thus leading to a lower cooling load for the CWAHEXs; thus, the heat obtained from the SAHEXs is more than is needed for the generation heat of the OAR to produce enough chilled water for the CWAHEXs. Once  $AT_{sahex}$  is higher than  $AT_{sahex,min}$  (dotted line in Figure 7,  $AT_{sahex} = 15$  °C), the cooling capacity of the SAHEXs drops, while the cooling load for the CWAHEXs increases until the heat obtained from the SAHEXs is insufficient to drive the OAR to cool the compressed air to the minimum suction temperature.  $ST_{com2}$  or  $ST_{com3}$  has to be enhanced alone or simultaneously with the increase in  $AT_{sahex}$ . Allowable  $AT_{sahex,max}$  corresponds to the working condition that  $ST_{com2}$  and  $ST_{com3}$  are both 40 °C.

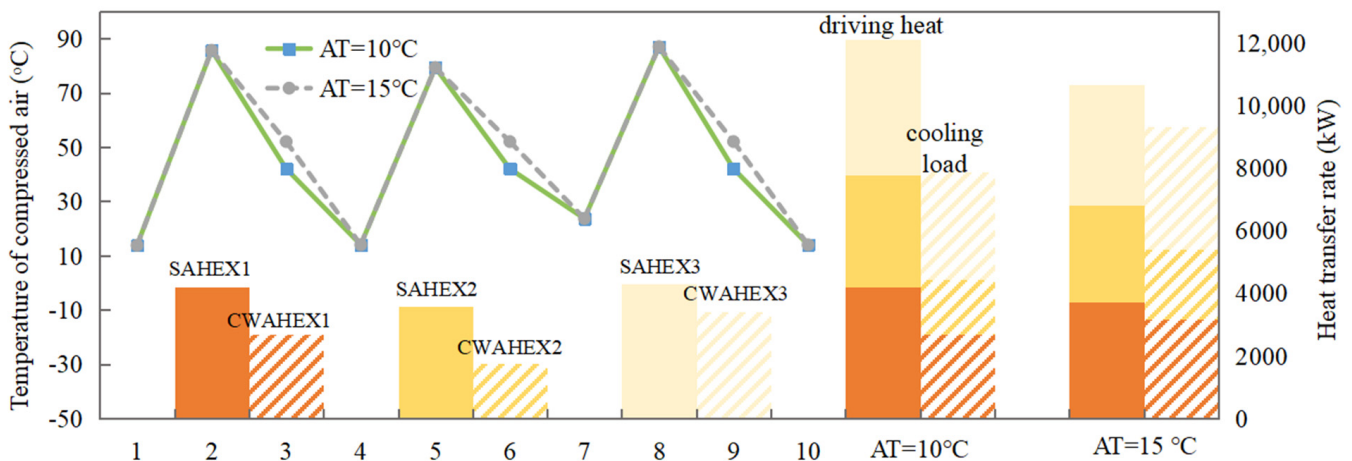
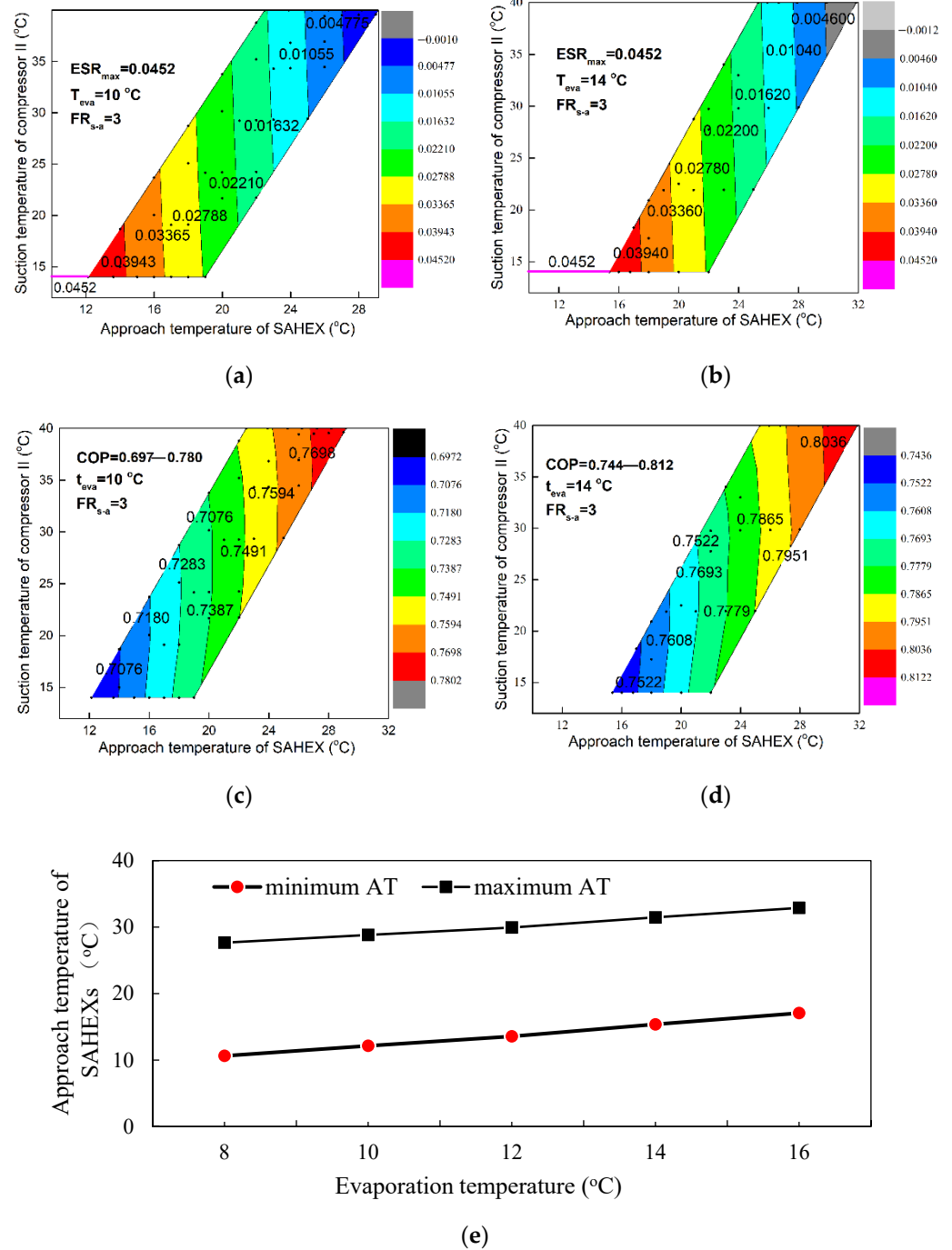


Figure 7. Cooling load allocation of SAHEXs and CWAHEXs.

Figures 6 and 7 also show that the allowable range of  $AT_{sahex}$  is closely related to  $T_{eva}$  and  $FR_{s-a}$ .  $AT_{sahex,min}$  and  $AT_{sahex,max}$  both increase with the increase in  $T_{eva}$  and  $FR_{s-a}$ . This result is supported by the fact that  $COP$  of OAR increases with a higher  $T_{eva}$  and  $FR_{s-a}$ , under which condition less generation heat is required by OAR for the same cooling load of the evaporator. This means that the heat allocation ratio between the SAHEXs and CWAHEXs can be decreased as a result of higher  $AT_{sahex,min}$  and  $AT_{sahex,max}$ . Based on the optimization of the suction temperatures of the compressors, the thermodynamic characteristics of the combined systems are analyzed below.

### 3.3. Parametric Analysis

To show the effect of operation parameters of the OAR on the system performance, we varied the  $AT_{sahex}$  from 8 to 32 °C,  $ST_{com2}$  and  $ST_{com3}$  from 14.01 to 40 °C and 23.66 to 40 °C, respectively, feed air temperature from 5 to 30 °C, and feed air humidity from 0 to 0.01 kg/kg. The corresponding  $ESR$  and  $COP$  at different  $T_{eva}$  and  $FR_{s-a}$  (Figure 8a–d) was then calculated.



**Figure 8.** Influence of evaporation temperature on *ESR* and *COP*: (a) *ESR* at  $T_{eva} = 10\text{ °C}$ ,  $FR_{s-a} = 3$ ; (b) *ESR* at  $T_{eva} = 14\text{ °C}$ ,  $FR_{s-a} = 3$ ; (c) *COP* at  $T_{eva} = 10\text{ °C}$ ,  $FR_{s-a} = 3$ ; (d) *COP* at  $T_{eva} = 14\text{ °C}$ ,  $FR_{s-a} = 3$ ; (e) minimum and maximum  $AT_{sahex}$  at different  $T_{eva}$ .

(1) Internal operating parameters

As shown in Figure 8a, *ESR* decreases as  $AT_{sahex}$  increases because either  $ST_{com2}$  or  $ST_{com3}$  has to be increased as  $AT_{sahex}$  increases. However, *ESR* only changes slightly with  $ST_{com2}$  due to the inverse relation between  $ST_{com2}$  and  $ST_{com3}$ . In other words, under a given working condition,  $AT_{sahex}$  almost plays a decisive role in the energy saving ratio. This is caused by the fact that *COP* does not change with  $AT_{sahex}$ , as shown in Figure 8c, which means the evaporation heat and generation heat ratio remains unchanged. However, energy allocation between SAHEXs and CWAHEXs changes with  $AT_{sahex}$ . Thus, the gross

heat of the SAHEXs and CWAHEXs has to be adjusted to maintain the energy allocation ratio to satisfy the evaporation heat and generation heat ratio; this is why  $ESR$  changes proportionally with  $AT_{sahex}$ . The change in the gross heat of the SAHEXs and CWAHEXs is implemented by the change in  $ST_{com2}$  and  $ST_{com3}$ ; considering the slight incline of the  $ESR$  line with the decrease in  $ST_{com2}$  (as shown in Figure 8a,b),  $ST_{com3}$  can be preferentially enhanced with the change in  $AT_{sahex}$ .

Comparing Figure 8a,b, the maximum  $ESR$  is the same for the different evaporation temperatures of the OAR system. However,  $ESR_{max}$  can only be reached at a designated  $AT_{sahex}$ . This further demonstrates that  $ESR$  is mainly affected by  $AT_{sahex}$  under a given humidity ratio of feed air and compression condition. As shown in Figure 8e, minimum and maximum  $AT_{sahex}$  increases proportionally with the increase in evaporation temperature. It can be concluded that a higher evaporation temperature permits a higher  $AT_{sahex}$ , which allows a smaller heat exchange area. From another perspective, for a given  $AT_{sahex}$ ,  $ESR_{max}$  increases with evaporation temperature.

It can be noted from Figure 8c,d that  $COP$  remains almost unchanged with  $AT_{sahex}$  and  $ST_{coms}$ , while it increases with the increase in  $T_{eva}$ .  $COP$  increases from 0.692 to 0.751 as  $T_{eva}$  increases from 12 to 14 °C.

To understand the effect of the solution flow ratio of the generator, we varied  $FR_{s-a}$  from 1 to 2.6. The maximum  $ESR$  predicted was 4.52%, as shown in Figure 9a,b, which further indicates that  $AT_{sahex}$  plays an almost exclusive role in the energy saving ratio at the given compression condition. As shown in Figure 9e, minimum and maximum  $AT_{sahex}$ , corresponding to the minimum  $ESR$  (0%) and maximum  $ESR$  (4.52%), firstly increase with the increase in solution flow ratio, whereafter, the increasing tendency gradually slows down as the flow ratio reaches above 2. The slowing down tendency is due to a limited generation efficiency, which reaches 94–97% when  $FR_{s-a}$  increases from 2.45 to 2.6. To achieve the maximum  $ESR$ , the allowable  $AT_{sahex}$  increases from 20.7–28.5 °C as  $FR_{s-a}$  increases from 1 to 2.6.

It can also be observed from Figure 9c,d that  $COP$  remains almost unchanged with the  $AT_{sahex}$  and  $ST_{coms}$ , while it decreases from 0.71 to 0.55 as  $FR_{s-a}$  reduces from 3 to 1.5. This is explained by the fact that the generation efficiency drops as  $FR_{s-a}$  reduces, which requires more fresh air for the regeneration of solution, leading to a larger air heating loss and consequent a lower  $COP$ .

## (2) External operating parameters

To demonstrate the energy saving potential of the coupled system, we further calculated the effect of climate conditions, mainly referring to the temperature and humidity ratio of the feed air, on the system performances.

During the calculation, we maximized the  $ESR$  by optimizing the approach temperature of SAHEX, while keeping the suction temperatures of compressor II and III as close as possible to the minimum suction temperatures. Figure 10a shows how  $ESR_{max}$  varies with the feed air temperature and humidity ratio.  $ESR_{max}$  increases with the decrease in air temperature and humidity ratio, whereas the growth tendency of  $ESR$  with the decrease in air humidity is more notable than that with air temperature. This is because the feed air temperature only has a direct influence on the energy consumption of compressor I, while feed air humidity ratio also indirectly influences the energy consumption of compressor II and III, due to its impact on the minimum suction temperature for each compressor. Maximum  $ESR$  reaches 8.045% when air temperature is 5 °C and the humidity ratio is 0.002 kg/kg. When air temperature and the humidity ratio increase above 30 °C and 0.01 kg/kg, the energy saving potential becomes insignificant. To achieve the maximum  $ESR$  for each temperature and humidity condition,  $AT_{sahex}$  has to be optimized, as shown in Figure 10c.

Under the maximum  $ESR$  case, the corresponding  $COP$  varies from 0.667 to 0.803. As can be observed from Figure 10b, there are turning points distributed on the iso-humid line of  $d = 0.0047$  kg/kg. The turning points occur because the evaporation temperature of OAR is set constantly as 12 °C when  $d > 0.0047$  kg/kg to satisfy the temperature demand for the molecular sieve, even though the minimum suction temperature of the compressors

is higher than 12 °C. Moreover,  $T_{eva}$  of OAR has to be adjusted according to the minimum suction temperature of compressor II, which is lower than 12 °C when  $d < 0.0047$  kg/kg, in order to satisfy the cooling demand of CWAHEX2. Therefore,  $COP$  decreases with the decrease in air humidity ratio below the turning point due to the decrease in  $T_{eva}$ .  $COP$  increases with the decrease in air humidity ratio above the turning point mainly because the required air for regeneration can be decreased as the air humidity ratio decreases (the air condition for regenerating is the same as the feed air), which further reduces the air heating loss and enhances  $COP$ . Though decreasing air heating loss is also applied for working conditions of  $d > 0.0047$  kg/kg, clearly, decreasing evaporation temperature plays a more critical role.

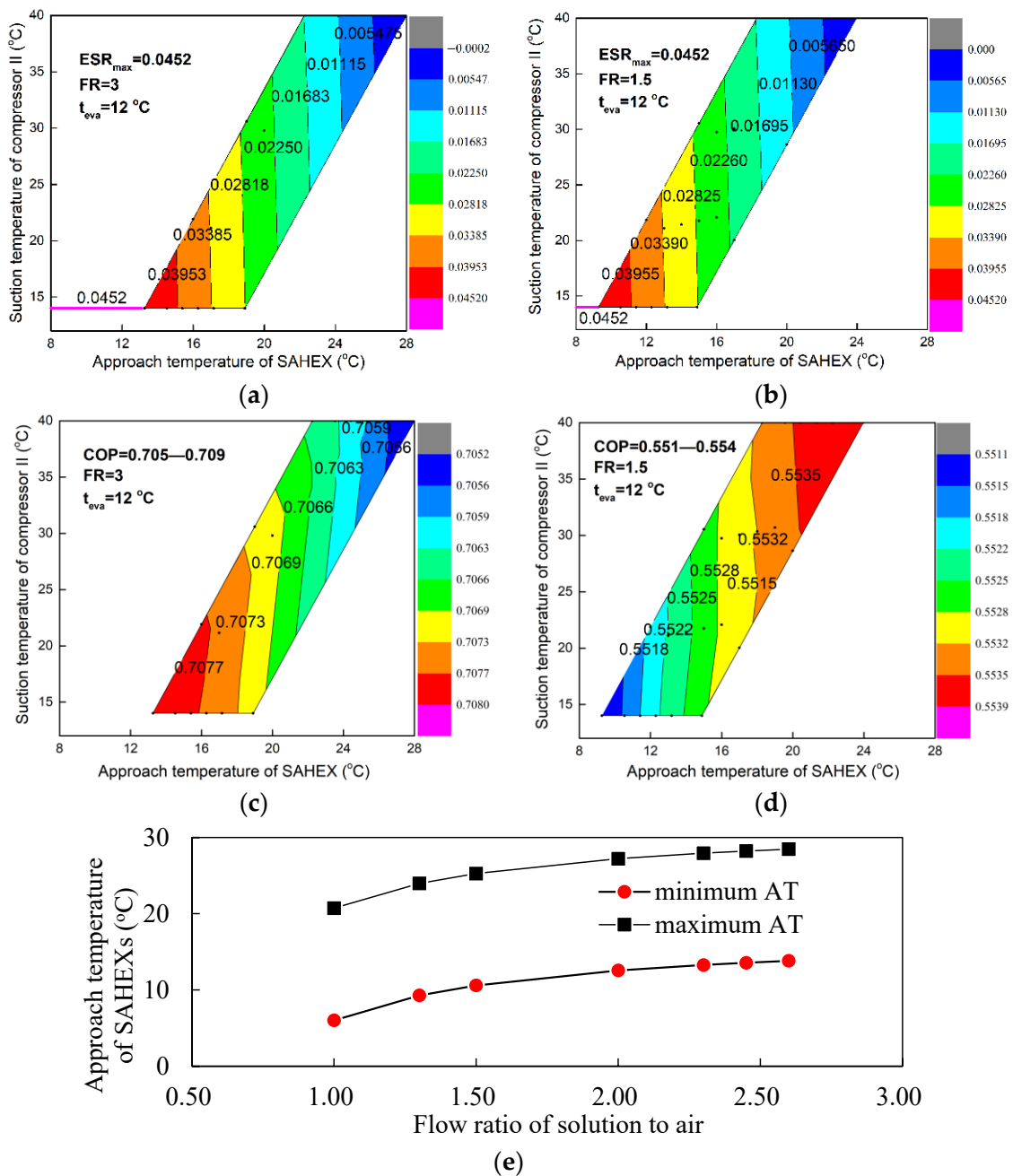


**Figure 9.** Influence of solution flow ratio on ESR and COP: (a) ESR at  $T_{eva} = 12$ ,  $FR_{s-a} = 3$ ; (b) ESR at  $T_{eva} = 12$ ,  $FR_{s-a} = 1.5$ ; (c) COP at  $T_{eva} = 12$ ,  $FR_{s-a} = 3$ ; (d) COP at  $T_{eva} = 12$ ,  $FR_{s-a} = 1.5$ ; (e) minimum and maximum  $AT_{sahex}$  at different  $FR_{s-a}$ .

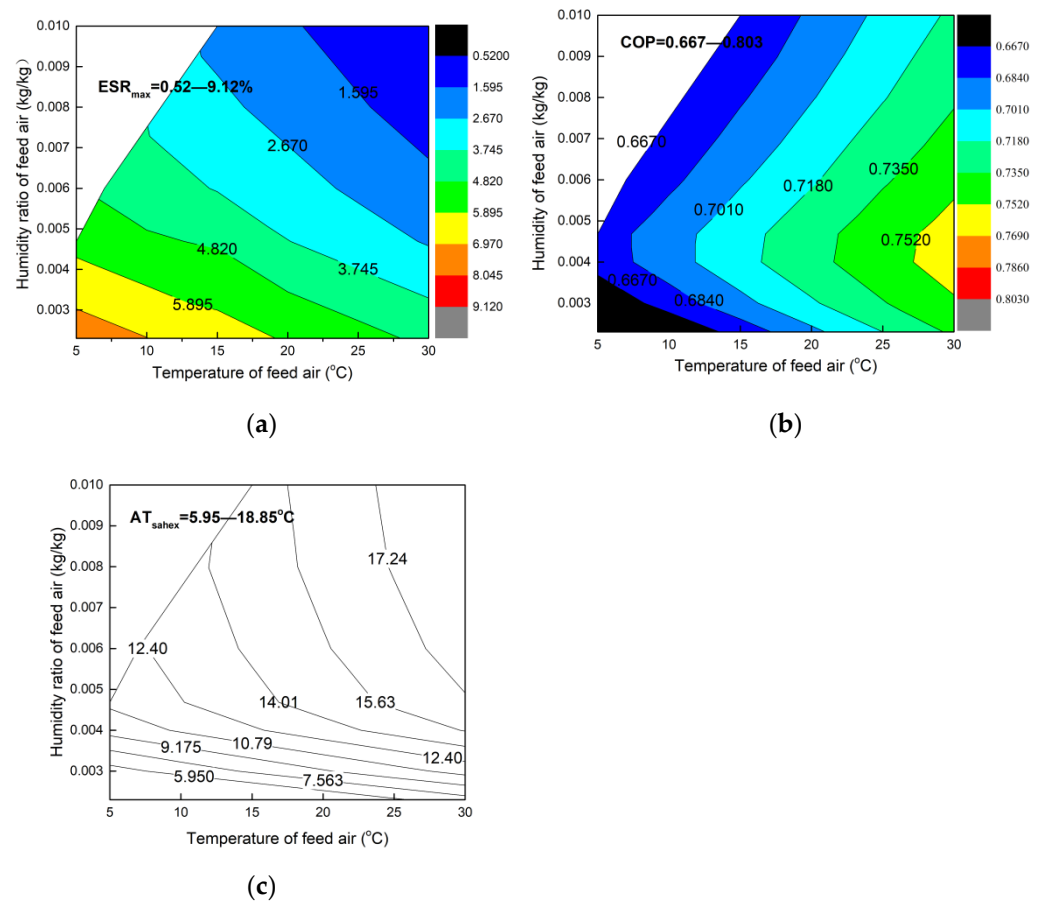


**Figure 10.** Influences of feed air temperature and humidity ratio on: (a) *ESR*; (b) *COP*; (c)  $AT_{sahex}$ .

### 3.4. Economic Analysis

Section 3.3 discusses effects of internal and external factors on the energy saving potential of the ACS–OAR system. We can tell that feed air temperature and humidity not only affect the *ESR* and *COP* of OAR directly, but also play a decisive role in the optimization of the approach temperature of heat exchangers, as well as the evaporation temperature and flow ratio of the generators, which is crucial for the initial cost and operation cost of the ACS–OAR system. We conducted an economic analysis under variable feed air working conditions in Beijing to demonstrate the profitability of the proposed system. Assumptions for the economic analysis are listed in Table 5.

**Table 5.** Assumptions for the economic analysis.

Parameters	Values
Life cycle of the system	25 year
Annual working hours	8000 h
Average electricity price	0.09 USD/kWh
Interest rate IR	8%
Discounted rate DR	2.5%
Tax rate	25%

According to Equation (37), *DPP* is directly related to project revenue (*Pr*) and cost of the OAR ( $C_{acs}$ ). While *Pr* is in direct proportion to *ESR*, which is almost exclusively determined by  $AT_{sahex}$ . Therefore, the key point to confirm *Pr* is the optimization of  $AT_{sahex}$ . As for the  $C_{acs}$ , it includes the capital cost of instruments, maintenance cost, management cost, and operating cost. The maintenance cost is set annually as 4.63% of the capital cost. The management cost is considered annually as 20% of the operating labor cost.

Compared to the operating of CASUs, workload for the operating of the OAR is relatively small; thus, additional labor cost is ignored. Additionally, no cost is obtained for heat source since the heat source for the OAR is the compression waste heat. Furthermore, the electricity consumption of the fans and pumps for intercoolers and ACTs in conventional ACSs can fully satisfy the electricity demand of the fans and pumps for the OAR. Thus, no additional operating cost is needed for the OAR. As the main equipment of the OAR are heat exchangers, the capital costs of the OAR are estimated by the heat transfer area, which is also strongly affected by the  $AT_{sahex}$ .

Considering the effects of  $AT_{sahex}$  on the two important variables ( $Pr$  and  $C_{acs}$ ) of  $DPP$ , designed  $AT_{sahex}$  will be optimized to achieve desirable economic evaluation indicators. Table 6 shows the monthly  $ESR$  calculated according to the variable feed air working conditions under different  $AT_{sahex}$ .

**Table 6.** Monthly energy saving ratio in Beijing.

Month	$T$ (°C)	$RH$ (%)	$D$ (kg/kg)	Original Electricity Consumption (kW)	$AT_{sahex}$									
					5	7	9	11	13	15	17	19	20	
					$ESR$ (%)									
1	−1.7	0.3	0.0001	19,872	7.01	6.84	6.49	6.12	5.85	5.34	4.61	4.87	4.49	
2	−0.7	0.39	0.0014	19,887	6.16	6.07	5.94	5.53	5.27	5.17	4.48	4.77	4.45	
3	9.7	0.31	0.0023	20,116	5.87	5.24	5.16	5.08	5	4.72	4.14	4.56	3.27	
4	14.7	0.43	0.0045	20,186	4.96	4.96	4.96	4.96	4.96	4.44	3.81	3.18	2.87	
5	22.3	0.38	0.0063	20,325	4.01	4.01	4.01	4.01	4.01	4.01	3.77	3.16	2.85	
6	26.3	0.51	0.0108	20,552	2.67	2.67	2.67	2.67	2.67	2.67	2.67	2.36	2.07	
7	28	0.62	0.0147	20,780	0	0	0	0	0	0	0	0	0	
8	25.9	0.60	0.0119	20,266	2.46	2.46	2.46	2.46	2.46	2.46	2.46	2.11	1.83	
9	23.1	0.58	0.0102	20,253	2.81	2.81	2.81	2.81	2.81	2.81	2.81	2.25	1.96	
10	13.3	0.59	0.0056	20,126	4.38	4.38	4.38	4.38	4.38	3.97	3.35	2.73	2.42	
11	5.8	0.52	0.0030	20,006	6.15	5.68	5.04	4.81	4.77	4.13	3.49	2.9	2.61	
12	−1.2	0.49	0.0017	19,878	6.41	6.02	5.92	5.23	5.03	4.59	4.25	3.6	3.28	
		annual average			4.41	4.26	4.15	4.01	3.93	3.69	3.32	3.04	2.68	

As can be seen from Table 6, the largest and smallest electricity consumption of conventional ACS occur in July and January, respectively. Conversely, the largest  $ESR$  (7.01%) occurs in January with  $AT_{sahex}$  at 5 °C, whereas  $ESR$  in July approaches approximately zero due to the high dewpoint temperatures of inhaled air at the inlets of second- and third-stage compressors, which are higher than 40 °C. In this condition, cooling produced by an OAR can still be supplied to the pre-cooling stage of compressed air before the molecular sieve stage. The annual average  $ESR$  of the ACS–OAR in Beijing is from 4.41% to 2.68%, as  $AT_{sahex}$  increases from 5 to 20 °C. Project revenue can be calculated based on  $ESR$  and electricity consumption values.

Direct capital cost of conventional cooling system is calculated based on the most unfavorable month, i.e., July, in which the heat transfer rates of intercoolers are the highest. The heat transfer area of OAR equipment corresponding to different  $AT_{sahex}$  was calculated. It is worth noting that heat transfer areas are not all based on the most unfavorable month, as a higher humidity of feed air in an unfavorable month permits a higher approach temperature. As shown in Figure 11, the annual cost of an OAR system, and project revenue, both increase with the decrease in  $AT_{sahex}$  of SAHEXs, while the increasing tendency of  $Pr$  is larger than that of  $C_{acs}$ . Thus, it can be speculated that the smallest  $DPP$  occurs in the largest  $Pr$ , as well as the largest  $ESR$  working condition. Table 7 lists the investment cost of components of OAR system and conventional cooling system. Indicators for economic analysis are also listed in Table 7. The direct capital cost of an OAR system ( $C_{dcc-oar}$ ) is USD 0.71 M while conventional cooling system costs USD 0.31 M. Thus, the net capital cost for the replacement of conventional cooling system by OAR ( $C_{dcc-oar-ccs}$ ) is USD 0.40 M. Annual operation, maintenance, and management cost for the OAR system are calculated as USD 0.07 M. Based on the  $C_{dcc-oar}$ , an  $NPV$  of USD 5.42 M can be obtained during the life cycle of the OAR system, with an estimated 1.32 year dynamic payback period. Based on  $C_{dcc-oar-ccs}$ , the  $NPV$  is calculated as USD 5.71 M, and the  $DPP$  is less than one

year (only nine months). From the above economic indicators, we can deduce that the OAR heat recovery system applied in the air compression section of the CASU shows great economic potential.

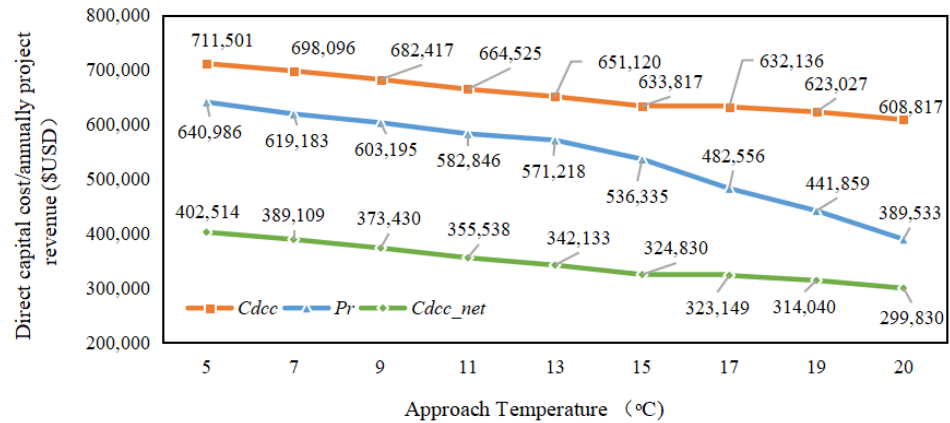


Figure 11. Influences of feed air temperature and humidity ratio on ESR and COP.

Table 7. Results of economic analysis.

Equipment	Design Parameters	Investment Cost (USD)
OAR system		711,501
SAHEX1	A = 295.4 m <sup>2</sup>	73,522
SAHEX2	A = 285.3 m <sup>2</sup>	71,871
SAHEX3	A = 253.7 m <sup>2</sup>	66,594
CWAHEX1	A = 198.1 m <sup>2</sup>	56,813
CWAHEX2	A = 293.1 m <sup>2</sup>	73,148
CWAHEX3	A = 191 m <sup>2</sup>	55,510
Absorber	A = 502.2 m <sup>2</sup>	104,477
Evaporator	A = 401.5 m <sup>2</sup>	79,991
Open generator	A = 424.3 m <sup>2</sup>	84,642
ACT1	Diameter = 3.5 m, Height = 3 m	19,533
Pump	Volume rate = 263.8 m <sup>3</sup> /h	16,538
Fan	Volume rate = 38.2 m <sup>3</sup> /s	8862
Annual operation, maintenance, and management cost		71,222
Conventional cooling system		308,988
Intercooler1	A = 328.69 m <sup>2</sup>	72,978
Intercooler2	A = 345.17 m <sup>2</sup>	75,557
Intercooler3	A = 383.09 m <sup>2</sup>	81,361
WCT	Diameter = 2.6 m, Height = 1.8 m	10,850
ACT1	Diameter = 3.7 m, Height = 3 m	19,640
ACT2	Diameter = 4 m, Height = 3.2 m	23,300
Pumps	Volume rate = 2844 m <sup>3</sup> /h	25,300
Annually project revenue (USD)	640,986	
NPV (USD)	5,423,691 (based on Capital cost of OAR) 5,709,802 (based on Net Capital cost of cooling system)	
DPP	1.32 year (based on Capital cost of OAR) 0.75 year (based on Net Capital cost of cooling system)	

#### 4. Conclusions

In this paper, an OAR system is proposed to be coupled with the air compression section in a cryogenic air separation unit. Due to its small temperature difference between the heat source and heat sink, the OAR system can reduce the compressed air to a relatively

low temperature by the close matching between its generation heat and cooling capacity. The close matching also makes it possible to realize the low evaporation temperature with a more simply structured OAR without external heat sinks. The coupling of the OAR system with the air compression section has been studied in this paper and proved to be technologically viable and profitable. The energy distribution principle and energy conversion principle between the multi-stage waste compression heat and cooling capacity of the OAR under different working conditions are discussed. The profitability is also analyzed.

The main conclusions are summarized below:

- (1) The distribution of cooling demand of compressed air, which corresponds to the cooling capacity of the SAHEXs and CWAHEXs of the OAR system, is crucial for the system balance and energy saving performance. Effects of operating parameters, including evaporation temperature, solution-to-air flow ratio, and the approach temperature of the SAHEXs, have been analyzed to illuminate the energy distribution and conversion principle. Ranges of approach temperatures of heat exchangers are optimized under different suction temperatures. The lower limit of approach temperature corresponds to the maximum ESR.
- (2) Feed air temperature and humidity ratio have a great impact on the system performance and energy saving potential. ESR ranges from 0.52–8.05%, corresponding to the temperature range of 5–30 °C and humidity range of 0.002–0.010 kg/kg. The annual mean energy saving ratio of the ACS–OAR reaches 4.41% based on the air condition in Beijing. A much higher ESR can be expected by installing a dehydrator before the compressors, as the present ESR is calculated based on a high suction temperature to avoid condensation water in the compressors.
- (3) Economic analysis has been conducted to estimate the capital cost, operation cost, and maintenance cost of the OAR system, as well as the net revenue, mainly referring to the electricity saving benefit caused by the coupling of OAR system. The payback period of OAR system is less than one year, and the net project revenue of OAR system during its life cycle reaches USD 5.7 M, showing attractive economic potential.

**Author Contributions:** Conceptualization, B.Y. and Z.W.; formal analysis, B.Y. and Z.W.; investigation and methodology, B.Y. and Z.W.; software, B.Y.; validation, S.S.; resources, Z.W.; data curation, S.S.; funding acquisition, B.Y. and Z.W. Project administration, Z.W.; Supervision, B.Y. and Z.W.; writing—original draft preparation, B.Y.; writing—review and editing, B.Y. and Z.W. All authors have read and agreed to the published version of the manuscript.

**Funding:** This research was funded by the Natural Science Foundation of Zhejiang Province, grant number LQ20E060011.

**Institutional Review Board Statement:** Not applicable.

**Data Availability Statement:** Not applicable.

**Conflicts of Interest:** The authors declare no conflict of interest. The funders had no role in the design of the study; in the collection, analyses, or interpretation of data; in the writing of the manuscript; or in the decision to publish the results.

## Nomenclature

### Nomenclature

A	area (m <sup>2</sup> )
C	cost (\$)
$c_p$	specific heat capacity (J/(kg·K))
d	absolute humidity of air, kg/kg;
dz	length of each segment respectively (m)
$D_h$	hydraulic diameter of flow channel
$D_f$	diffusivity coefficient (m <sup>2</sup> /s)
$D_r$	discounted annual rate
h	enthalpy (kJ/kg)

i	sequence of the element indices
K	overall mass transfer coefficient (kg/(m <sup>2</sup> ·s))
$k_{air}^i$	air side mass transfer coefficient (kg/(m <sup>2</sup> ·s))
$k_m$	permeability of the membrane (kg/(m·s))
m	mass flow rate (kg/s)
P	pressure (kPa)
$P_r$	project revenue
$p_v$	water vapor partial pressure (kPa)
Q	heat transfer rate (kW)
R	ideal gas constant (J/(mol·K))
$r_c$	compression ratio (%)
T	temperature (K)
t	temperature (°C)
$T_r$	tax rate
U	overall heat transfer coefficient (W/(m <sup>2</sup> ·K))
$u_a$	air side heat transfer coefficient (W/(m <sup>2</sup> ·K))
$u_s$	solution side heat transfer coefficient (W/(m <sup>2</sup> ·K))
W	power consumption (kW)
x	mass fraction of solvent in the solution (%)
$\eta_{comp}$	isentropic efficiency of compressors (%);
$\varepsilon$	heat transfer effectiveness (%)
$\eta_{sp}$	solution pump efficiency (%)
$\lambda$	thermal conductivity of membrane (W/(m·K))
$\theta_m$	thickness of membrane (m)

#### Abbreviations

ACS	air compression section
ACT	air-cooling tower
AR	absorption refrigerator
ASU	air separation unit
CAR	close absorption refrigerator
CASU	cryogenic air separation unit
COP	Coefficient of performance
CWAHEX	cooling water-air heat exchanger
DPP	dynamic payback period
ESR	energy saving ratio
EP	electricity purchase price.
LNG	liquefied natural gas
NPV	net present value
NTU	number of transfer unit
ORC	organic Rankine cycle
OAR	open absorption refrigerator
SAHEX	solution-air heat exchanger
VFMD	vacuum fiber membrane dehumidification
VCR	vapor compression refrigerator
WCT	water-cooling tower
WHRR	waste heat recovery ratio
wh	working hours of the system

#### References

1. Industry Research Report of Industrial Gas in China. Available online: [https://www.djyanbao.com/preview/2986401?from=search\\_list](https://www.djyanbao.com/preview/2986401?from=search_list) (accessed on 1 January 2022).
2. Tong, L.G.; Zhang, A.J.; Li, Y.L.; Yao, L.; Wang, L.; Li, H.; Li, L.; Ding, Y. Exergy and energy analysis of a load regulation method of CVO of air separation unit. *Appl. Therm. Eng.* **2015**, *80*, 413–423. [CrossRef]
3. Singla, R.; Chowdhury, K. Comparisons of thermodynamic and economic performances of cryogenic air separation plants designed for external and internal compression of oxygen. *Appl. Therm. Eng.* **2019**, *160*, 114025. [CrossRef]
4. Pintilie, M.; Erban, A.; Popa, V.; Popa, C.L. Design analysis of low pressure distillation column for cryogenic air separation. *IOP Conf. Ser. Mater. Sci. Eng.* **2019**, *595*, 012023. [CrossRef]
5. Xu, J.H.; Wang, T.; Chen, Q.; Zhang, S.; Tan, J. Performance design of a cryogenic air separation unit for variable working conditions using the lumped parameter model. *Front. Mech. Eng.* **2020**, *15*, 19–26. [CrossRef]
6. Rong, Y.; Zhi, X.; Wang, K.; Zhou, X.; Cheng, X.; Qiu, L.; Chi, X. Approach to the method to utilize the low-grade residual compression heat during the air separation process. *Cryog. Technol.* **2019**, *1*, 5–12.

7. Wu, Y.; Xiang, Y.; Cai, L.; Liu, H.; Liang, Y. Optimization of a novel cryogenic air separation process based on cold energy recovery of LNG with exergoeconomic analysis. *J. Clean. Prod.* **2020**, *275*, 123027. [[CrossRef](#)]
8. Ebrahimi, A.; Ziabasharhagh, M. Optimal design and integration of a cryogenic Air Separation Unit (ASU) with Liquefied Natural Gas (LNG) as heat sink, thermodynamic and economic analyses. *Energy* **2017**, *12*, 868–875. [[CrossRef](#)]
9. Rong, Y. Design Optimization and Experimental Research of Self-Enhancement Multi-Stage Air Compression Process Driven by Heat Recovery in Air Separation Units. Ph.D. Thesis, Zhejiang University, Hangzhou, China, 2021.
10. Lou, H.F.; Li, Y.J.; Shao, Z.J. Dynamic processes of cryogenic air separation distillation systems: A review. *J. Chem. Eng. Chin. Univ.* **2019**, *33*, 775–785.
11. Tian, Q.Q. A Study on Modeling Large-Scale Air Separation Units and Low Energy Consumption. Ph.D. Thesis, Huazhong University of Science and Technology, Wuhan, China, 2016.
12. Saidur, R.; Rahim, N.A.; Hasanuzzaman, M. A review on compressed-air energy use and energy savings. *Renew. Sustain. Energy Rev.* **2010**, *14*, 1135–1153. [[CrossRef](#)]
13. Zhu, S.; Zhang, K.; Deng, K. A review of waste heat recovery from the marine engine with highly efficient bottoming power cycles. *Renew. Sustain. Energy Rev.* **2020**, *120*, 109611. [[CrossRef](#)]
14. Aneke, M.; Wang, M. Potential for improving the energy efficiency of cryogenic air separation unit (ASU) using binary heat recovery cycles. *Appl. Therm. Eng.* **2015**, *81*, 223–331. [[CrossRef](#)]
15. Zhang, T.; Zhang, X.L.; He, Y.L.; Xue, X.D.; Mei, S.W. Thermodynamic analysis of hybrid liquid air energy storage systems based on cascaded storage and effective utilization of compression heat. *Appl. Therm. Eng.* **2020**, *164*, 114526. [[CrossRef](#)]
16. Teng, S.Y.; Wang, M.W.; Xi, H.; Wen, S.Q. Energy, exergy, economic (3E) analysis, optimization and comparison of different ORC based CHP systems for waste heat recovery. *Case Stud. Therm. Eng.* **2021**, *28*, 101444. [[CrossRef](#)]
17. Yu, H.S.; Eason, J.; Biegler, L.T.; Feng, X.; Gundersen, T. Process optimization and working fluid mixture design for organic Rankine cycles (ORCs) recovering compression heat in oxy-combustion power plants. *Energy Convers. Manag.* **2018**, *175*, 132–141. [[CrossRef](#)]
18. Li, Y.; Zhou, P.; Zhuang, Y.; Wu, X.; Liu, Y.; Han, X.; Chen, G. An improved gas leakage model and research on the leakage field strength characteristics of R290 in limited space. *Appl. Sci.* **2022**, *12*, 5657. [[CrossRef](#)]
19. Zheng, Z.Y.; Cao, J.Y.; Wu, W.; Michael, K.H.L. Parallel and in-series arrangements of zeotropic dual-pressure Organic Rankine Cycle (ORC) for low-grade waste heat recovery. *Energy Rep.* **2022**, *8*, 2630–2645. [[CrossRef](#)]
20. Rong, Y.; Wu, Q.X.; Zhou, X.; Fang, S.; Wang, K.; Qiu, L.; Zhi, X. Research on optimization of self-utilization performance of air compression waste heat in air separation system. *CIESC J.* **2021**, *72*, 13–21.
21. Rong, Y.; Zhi, X.; Wang, K.; Zhou, X.; Cheng, X.; Qiu, L.; Chi, X. Thermoeconomic analysis on a cascade energy utilization system for compression heat in air separation units. *Energy Convers. Manag.* **2020**, *213*, 112820. [[CrossRef](#)]
22. Zhou, X.; Rong, Y.; Fang, S.; Wang, K.; Zhi, X.; Qiu, L.; Chi, X. Thermodynamic analysis of an organic Rankine-vapor compression cycle (ORVC) assisted air compression system for cryogenic air separation units. *Appl. Therm. Eng.* **2021**, *189*, 116678. [[CrossRef](#)]
23. Mao, J.; Chen, G.; Ren, Z. Thermoelectric cooling materials. *Nat. Mater.* **2021**, *20*, 454–461. [[CrossRef](#)]
24. Chen, W.Y.; Shi, X.L.; Zou, J.; Chen, Z.G. Thermoelectric coolers: Progress, Challenges, and Opportunities. *Small Methods* **2022**, *6*, 2101235. [[CrossRef](#)]
25. Rahman, S.M.A.; Hachicha, A.A.; Ghenai, C.; Saidur, R.; Said, Z. Performance and life cycle analysis of a novel portable solar thermoelectric refrigerator. *Case Stud. Therm. Eng.* **2020**, *19*, 100599. [[CrossRef](#)]
26. Mansour, K.; Qiu, Y.; Hill, C.J.; Soibel, A.; Yang, R.Q. Mid-infrared interband cascade lasers at thermoelectric cooler temperatures. *Electron. Lett.* **2006**, *42*, 1034–1036. [[CrossRef](#)]
27. Huang, B.; Shen, Z.G. Performance assessment of annular thermoelectric generators for automobile exhaust waste heat recovery. *Energy* **2022**, *246*, 123375. [[CrossRef](#)]
28. Zhu, X.L.; Zhao, J.; Wu, Y.T.; He, X.L.; Jia, H.L. Dehumidification system for air compressor suction end and waste heat utilization of lubricating oil. *Build. Energy Effic.* **2017**, *8*, 101–104.
29. Du, F.J. Study on the Refrigeration and Use of Interstage Gas's Waste Heat of Nitrogen-Hydrogen Compressor. Ph.D. Thesis, Zhengzhou University, Zhengzhou, China, 2013.
30. Zhi, X.; Zhou, X.; Rong, Y.; Li, J.F.; Cheng, X.W.; Qiu, L.M. An Air Separation System with Waste Compression Heat Recovery. CN201710995255.X, 23 October 2017.
31. Wang, R.Z.; Wang, L.W.; Cai, J.; Du, S.; Hu, B.; Pan, Q.W.; Jiang, L.; Xu, Z.Y. Research status and trends on industrial heat pump and network utilization of waste heat. *J. Refrig.* **2017**, *38*, 1–10. [[CrossRef](#)]
32. El-Shafei, B.Z.; Ayman, A.A.; Ahmed, M.H. Modeling and simulation of solar-powered liquid desiccant regenerator for open absorption cooling cycle. *Sol. Energy* **2011**, *85*, 2977–2986.
33. Ayman, A.A.; El-shafei, B.Z.; Ahmed, M.H. Performance evaluation of open-cycle solar regenerator using artificial neural network technique. *Energy Build.* **2011**, *43*, 454–462.
34. Ye, B.C.; Wang, Z.; Yan, X.N.; Chen, G.M. Performance analysis of a variable-stage open absorption heat pump combined with a membrane absorber. *Energy Convers. Manag.* **2019**, *184*, 290–300. [[CrossRef](#)]
35. Cost Engineering: Equipment Purchase Costs. Available online: <https://www.chemengonline.com/cost-engineering-equipment-purchase-costs/> (accessed on 1 January 2019).

36. Rahimi, S.; Meratizaman, M.; Monadizadeh, S.; Amidpour, M. Techno-economic analysis of wind turbineePEM (polymer electrolyte membrane) fuel cell hybrid system in standalone area. *Energy* **2014**, *67*, 381–387. [[CrossRef](#)]
37. Sayyaadi, H.; Mehrabipour, R. Efficiency enhancement of a gas turbine cycle using an optimized tubular recuperative heat exchanger. *Energy* **2012**, *38*, 362–369. [[CrossRef](#)]
38. Wei, Z.; Zhang, B.; Wu, S.; Chen, Q.; Tsatsaronis, G. Energy-use analysis and evaluation of distillation systems through avoidable exergy destruction and investment costs. *Energy* **2012**, *42*, 424–430. [[CrossRef](#)]